ACS APPLIED MATERIALS & INTERFACES

Research Article

www.acsami.org

Enhancement of VEGF-Mediated Angiogenesis by 2-*N*,6-*O*-Sulfated Chitosan-Coated Hierarchical PLGA Scaffolds

Yuanman Yu,[†,§] Jie Chen,[†,§] Rui Chen,[†,§] Lingyan Cao,[†,§] Wei Tang,[†,§] Dan Lin,[†,§] Jing Wang,*[,†,§] and Changsheng Liu*[,†,‡,§]

[†]The State Key Laboratory of Bioreactor Engineering, [‡]Key Laboratory for Ultrafine Materials of Ministry of Education, [§]Engineering Research Center for Biomedical Materials of Ministry of Education, East China University of Science and Technology, Shanghai 200237, People's Republic of China

ABSTRACT: Rapid and controlled vascularization within scaffolds remains one of the key limitations in tissue engineering applications. This study describes the fabrication and characterization of 2-*N*,6-*O*-sulfated chitosan (26SCS)-coated hierarchical scaffold composed of poly(lactic-*co*-glycolic acid) (PLGA) microspheres, as a desirable vehicle for vascular endothelial growth factor (VEGF) delivery and consequent angiogenic boosting *in vitro*. Owing to the hierarchical porous structure and high affinity between VEGF and 26SCS, the 26SCS-modified PLGA (S-PLGA) scaffold possesses excellent entrapment and sustained release of VEGF. Using human umbilical vein endothelial cells (HUVECs) as a cell model, the VEGF-loaded S-PLGA scaffold shows desirable cell viability and attachment. The bioactivity of released VEGF is validated by intracellular nitric oxide secretion and capillary tube formation, demonstrating the improved capacity of VEGF-mediated pro-angiogenesis ascribed to 26SCS incorporation. Such a strategy will afford an effective method to prepare a scaffold with promoted angiogenesis.

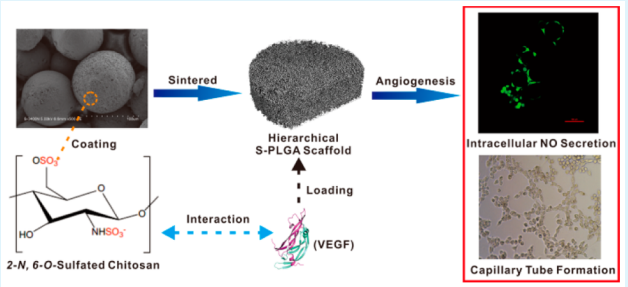

KEYWORDS: *scaffold, poly(lactic-co-glycolic acid), sulfated chitosan, vascular endothelial growth factor, angiogenesis*

1. INTRODUCTION

Tissue engineering is one of the most promising approaches to treat wound healing and tissue regeneration.[1,2] However, the vascularization of engineered constructs is still a significant challenge due to a deficiency of blood vessels that can provide oxygen and nutrients to sustain cell viability.[3,4] To address this problem, many strategies have been employed: delivering pro-angiogenic growth factors, such as encapsulation, adsorption, ion complexation, or covalent immobilization in a carrier matrix,[5−7] endows the potential angiogenic capability; modulating structural parameters, such as scaffold porosity, avails the transmission of nutrition, as well as cellular adhesion and migration.[8,9] Yet, thus far, the suitable strategy to develop sufficient vasculature has not been identified.

Angiogenic processes are regulated by various growth factors, among which vascular endothelial growth factor (VEGF) holds the greatest potential to promote endothelial cells proliferation, migration, survival, and angiogenesis *in vitro*, as well as the formation of new blood vessels *in vivo*.[10,11] However, soluble VEGF is quickly degraded by enzymes in the body or undergo other physical and chemical denaturations that shorten its biological half-life.[12] Previous studies using intravenously injected VEGF showed that the protein has a half-life of less than 1 h.[13] As a result, current clinical applications require a high dose of VEGF which is often associated with severe side effects including vasodilation, hypertension, inappropriate blood vessels growth, atherosclerotic plaque development, and neovascularization of tumors.[14,15] Therefore, a delivery system with the ability of controlling VEGF localization and release behavior becomes imperative. Incorporation of VEGF into scaffolds or microspheres has shown the potential for local delivery at a more controllable releasing rate. Unfortunately, current techniques to encapsulate and protect of VEGF often involve harsh organic solvents, which decreases the loading amount and biological activity of the protein.

Meanwhile, recent findings in developmental biology provide compelling evidence that heparin, a highly sulfated glycosaminoglycan in extracellular matrix, can provide optimal balance between diffusion and retention of VEGF.[16−18] Heparin presents specific motifs with negatively charged sulfate groups which can help tightly bind to growth factors via electrostatic interaction and thus limit their diffusion. Heparin also has a relatively longer half-life (about 90 min) than VEGF, and consequently preserves the bioactivity of bound VEGF against thermolysis and enzymolysis.[19,20] However, opposing viewpoints claim that a high concentration of exogenous heparin is associated with hemorrhage, thrombocytopenia, osteoporosis, and anaphylactoid-type reactions.[21−23] Therefore, seeking a substance which retains the effects of heparin and avoids its side effects becomes necessary. More recently,

Received: March 16, 2015
Accepted: April 23, 2015
Published: April 23, 2015

ACS Publications © 2015 American Chemical Society

DOI: 10.1021/acsami.5b02324
ACS Appl. Mater. Interfaces 2015, 7, 9982−9990

Scheme 1. Schematic Diagram of the Preparation Process of 26SCS-Coated Hierarchical PLGA Scaffold and the Combinatorial Effect of Hierarchical Structure and 26SCS on VEGF Mediated Angiogenesis *in Vitro*[a]

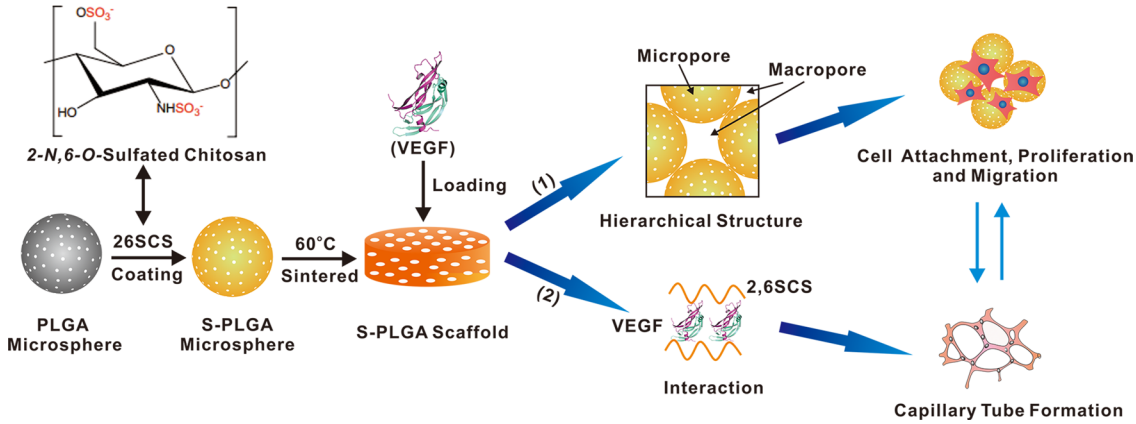

[a](1) Interconnected hierarchical structure and hydrophilic-modified interface of the scaffold favored cell attachment, proliferation, and migration. (2) Better binding efficiency and sustained releasing dynamics were acquired owing to the interaction between 26SCS and VEGF, which further stimulated the intracellular nitric oxide (NO) expression and capillary tube formation, indicated the enhanced pro-angiogenesis capability.

sulfated chitosan as a kind of heparin-like polysaccharide has attracted popular interests for its structure similarity with heparin and higher sulfation degree than any natural sulfated polysaccharides, while 2-*N*,6-*O*-sulfated chitosan (26SCS) stands out of the crowd. Furthermore, our previous study has demonstrated that 26SCS could efficiently promote vessel formation during bone regeneration.[24] Therefore, we hypothesize that 26SCS not only can serve as a conjugate that prolongs the bioactivity of VEGF but also has the potential of synergizing with VEGF to promote angiogenesis.

Herein, a mild and facile strategy of preparing a 26SCS-mediated VEGF delivery system was developed. Biodegradable poly(lactic-*co*-glycolic acid) (PLGA) was selected as the matrix for its good biocompatibility, mechanical strength, and adjustable degradation rate, which had been approved by FDA for tissue engineering and drug delivery.[25−27] Nevertheless, poor hydrophilicity, low loading efficiency, and unpredictable release behaviors with high initial bursts astrict its further development.[28] Thereupon, three-dimensional (3D) scaffolds with interconnected and hierarchical structure were fabricated through a sintering process of 26SCS-coated porous PLGA microspheres. The microsphere-based scaffolds were characterized by scanning electron microscopy (SEM) and synchrotron radiation-based microcomputed tomography (SRμCT) imaging for morphology and porosity determination, respectively. In addition, 26SCS distribution on the scaffold was visualized with toluidine blue staining and further confirmed by X-ray photoelectron spectroscopy (XPS). As a delivery vehicle for active growth factor, the release behavior of VEGF from scaffolds as well as the angiogenic potentials was examined *in vitro*. We hypothesized that PLGA scaffolds with hierarchical structure not only were beneficial for cell nutrition, proliferation, and migration, which made for vascularization and formation of new tissue, but also improve the entrapment efficiency of VEGF. Furthermore, introduction of 26SCS regulates the release behavior of VEGF through interaction between heparin-like polysaccharides and growth factors and achieves more effective pro-angiogenesis capability of VEGF (Scheme 1).

2. MATERIALS AND METHODS

2.1. Materials. Poly(lactic-*co*-glycolic acid) with a 50:50 monomer ratio and average molecular weight of 100 kDa was purchased from Jinan Dai Gang Biological Technology Co., Ltd. (Jinan, China). Toluidine blue zinc chloride double salt, 3-(4,5-dimethylthiazol-2-yl)-2,5-diphenyltetrazolium bromide (MTT), poly(vinyl alcohol) (PVA; M_w 13,000−23,000; 87−89% hydrolyzed), fluorescein isothiocyanate-phalloidin (FITC-phalloidin), triblock copolymer Pluronic F127 ($EO_{106}PO_{70}EO_{106}$ with EO = ethylene oxide and PO = propylene oxide; 99.0 wt %) were obtained from Sigma-Aldrich (St. Louis, MO, USA). Recombinant human VEGF was purchased from PeproTech (Rocky Hill, NJ, USA). Growth factor reduced Matrigel Matrix was from BD Biosciences (San Jose, CA, USA). All cell-culture-related reagents were available from Gibco (Grand Island, NY, USA).

2.2. Preparation of Porous PLGA Microsphere. Porous PLGA microspheres were prepared through emulsion method by using Pluronic F127 as an extractable porogen. A 300 mg amount of PLGA and 700 mg of Pluronic F127 were dissolved in 3 mL of methylene chloride. The polymer solution was then added dropwise into 100 mL of 0.5% PVA aqueous solution (w/v) under 1000 rpm vortex at room temperature. The resultant emulsion was placed in a ventilated hood under stirring for 12 h to evaporate methylene chloride, followed by centrifugation to achieve microspheres. The microspheres were washed with deionized water and ethanol for three times respectively to remove PVA and F127 and then lyophilized to achieve the porous PLGA microspheres.

2.3. Functionalization of Porous PLGA Microspheres with 2-*N*,6-*O*-Sulfated Chitosan. In this study, a surface adsorption method was adopted to fabricate functional porous PLGA microspheres. 26SCS was prepared as previously described.[29] Briefly, 26SCS was dissolved in deionized water to obtain a 0.1% 26SCS solution (w/v). The porous microspheres were immersed in the freshly prepared 26SCS solution and saturated for 4 h at room temperature, then centrifuged and washed with deionized water repeatedly to remove the redundant 26SCS. The harvested products were lyophilized to obtain the 26SCS-coated PLGA microspheres. The unmodified microspheres and modified microspheres will be referred to as PLGA microspheres and S-PLGA microspheres, respectively.

2.4. Fabrication of Hierarchical PLGA Scaffolds. To fabricate PLGA microsphere accumulated scaffolds, PLGA microspheres and S-PLGA microspheres were dispersed into a Teflon mold (Φ 8 mm × 5 mm) and heated at 60 °C for 30 min. After being cooled to room temperature, the samples were demolded and the resulting scaffolds were stored in a desiccator for further application. Scaffolds consisting of unmodified and 26SCS-modified porous PLGA microspheres will be referred to as PLGA and S-PLGA scaffolds, respectively.

DOI: 10.1021/acsami.5b02324
ACS Appl. Mater. Interfaces 2015, 7, 9982−9990

2.5. Morphology Observation. The obtained microspheres and scaffolds were morphologically characterized by scanning electron microscopy (SEM; S-3400, Hitachi, Tokyo, Japan). The uniformly dispersed microspheres and the cross-sections of the scaffolds were sputter-coated with gold before scanning.

In an attempt to explore the 3D microstructure of the scaffolds, synchrotron radiation based microcomputed tomography (SRμCT) measurement was performed at the BL13W beamline of the Shanghai Synchrotron Radiation Facility (SSRF, Shanghai, China) using a monochromatic beam with energy of 20 keV and a sample-to-detector distance of 0.5 m. In the current study, a 2048 × 2048 sCMOS detector (Flash 4.0, Hamamatsu, Hamamatsu City, Japan) with the pixel size set to 9 μm was used to record tomographies. Within an angular range of 180°, 1080 projections were taken and the exposure time amounted to 1 s per projection. Slice images were reconstructed using a filtered back-projection algorithm, and were finally re-digitized with an 8-bit data format. The VG Studio MAX 2.1 software (Volume Graphics, Heidelberg, Germany) served for the visualization of the 3D structure from slice images. The 3D void volume percentages were calculated as scaffold porosities.

2.6. X-ray Photoelectron Spectroscopy Analysis. The surface chemical compositions of PLGA and S-PLGA (ESCALAB 250Xi , Thermo Scientific , Waltham, MA, USA) microspheres were investigated by XPS (PH1500C) equipped with argon ion gun. The elements presented on the sample surface were identified from a survey spectrum recorded over the energy range of 0−1400 eV and a resolution of 1.0 eV. For further analysis, high-resolution spectra were recorded from pertinent photoelectron peaks to identify the chemical state of each element. The atomic concentration of each element was calculated by determining the relevant integral peak intensities. All of the binding energies (BEs) were referenced to the C 1s neutral carbon peak at 285 eV to compensate for surface charging.

2.7. Toluidine Blue Staining and Assay. The coating of 26SCS on scaffolds was visualized by toluidine blue (TB) staining.[30] The PLGA and S-PLGA scaffolds were incubated for 6 h in TB solution (aqueous solution containing 0.005% (w/v) toluidine blue zinc chloride double salt, 0.01 M hydrochloric acid, and 0.2% (w/v) sodium chloride) at room temperature. The purple color developed on scaffolds indicated the presence of immobilized 26SCS.

The 26SCS content in the scaffolds was quantified by TB assay. Freeze-dried scaffolds were immersed in a 1 mL solution of chloroform/acetone (1:1 (v/v) ratio). The suspension was vortexed and centrifuged at 12000*g* for 15 min. 26SCS was washed twice with chloroform/acetone solution. The remanent organic solvent was allowed to evaporate, and 26SCS was immersed in 1 mL of TB solution for 3 h. Subsequently, an equal volume of *n*-hexane was added. The absorption of TB solution was measured at 630 nm using a plate reader according to a standard curve of 26SCS with known concentrations. Meanwhile, quantitative examination was implemented to detect the release of 26SCS from scaffolds at 12, 24, and 48 h, respectively. Cumulative release is expressed as a percentage of total adsorbed 26SCS.

2.8. Contact Angle Measurements. Sessile drop water contact angles were used to determine the hydrophilicity of PLGA and S-PLGA scaffolds. Sessile drops, 1 μL each, were produced by pushing distilled water out of a needle in close proximity to the substrate. Measurements were taken after 20 s of equilibration. The data were recorded using a digital camera (Nikon, Tokyo, Japan).

2.9. *In Vitro* Adsorption and Release of VEGF. For adsorption determination, scaffolds were immersed in 1 mL of phosphate-buffered saline (PBS) containing VEGF (500 ng, 1 μg/mL in 0.1% bovine serum albumin (BSA) aqueous solution). During incubation, scaffolds were stirred moderately at 37 °C. The supernatants were collected after 24 h; then the VEGF bound to the scaffolds were washed with PBS for three times. All of the washing liquid was also collected. The concentrations of VEGF in the collected solutions were assayed using a Human VEGF ELISA kit (Neobioscience Technology, Shanghai, China) according to the manufacturer's instructions. The VEGF adsorption of the scaffolds is evaluated by binding efficiency, which is expressed as a percentage of the total added protein.

To study the release behavior, PLGA and S-PLGA porous scaffolds were put into 24-well plates. The solution of VEGF was blotted onto each sample (50 ng of VEGF per sample) in sterile conditions and stayed for 4 h to be totally absorbed, named as PLGA/VEGF and S-PLGA/VEGF scaffolds, respectively. Then the VEGF-loaded scaffolds were lyophilized and stored at −20 °C for releasing inspection. The amount of VEGF released from the scaffolds was quantified over a period of 96 h using a Human VEGF ELISA kit according to the manufacturer's instructions. Briefly, the VEGF-loaded samples were put into 1 mL of PBS in a 24-well plate at 37 °C in a humidified atmosphere of 5% CO_2. The release buffer was collected at specified time points and replenished using an equal volume of fresh buffer. This analysis was performed in triplicate. Cumulative release is expressed as a percentage of the total loaded protein.

2.10. *In Vitro* Angiogenesis Evaluation. *2.10.1. Cell Viability.* Human umbilical vein endothelial cells (HUVECs; purchased from the American Type Culture Collection) were seeded onto VEGF-loaded PLGA and S-PLGA scaffolds at a density of 2 × 10^4 cells/mL and incubated in Dulbecco's modified Eagle's medium (DMEM) with 10% fetal bovine serum (FBS) and 1% penicillin−streptomycin at 37 °C, 5% CO_2, in a humidified environment. Cells cultured directly on a 24-well plate with only culture medium and fresh VEGF were set as the negative control and positive control, respectively. Medium was changed every 3 days. After 1, 3, and 7 days, the cell viability was evaluated with MTT assay. In brief, samples were placed in a culture medium containing MTT, which was further incubated in a humidified atmosphere at 37 °C for 4 h. Optical density (OD) of the resulting solution of each sample was measured at 492 nm using a microplate reader. Results were reported as the percentage ratio of $OD_{sample}/OD_{negative\ control\ (1\ d)}$ × 100% (n = 5). Cell viability was visualized using a live/dead assay kit (Abcam, Cambridge, U.K.) after HUVECs culturing on scaffolds for 24 h following the standard protocol provided by the manufacturer. Briefly, cells and scaffolds were first washed twice with PBS and then incubated in standard working reagent at 37 °C for 15 min. The PLGA/VEGF and S-PLGA/VEGF scaffolds were then washed twice with PBS and studied under the confocal laser scanning microscopy (CLSM; Nikon A1R, Nikon).

2.10.2. Cell Adhesion and Morphology. HUVECs were seeded onto PLGA and S-PLGA scaffolds in a 24-well plate at a density of 5.0 × 10^4 cells/mL. After 12 h incubation, samples were washed with PBS twice and fixed with 2.5% glutaraldehyde for 15 min. The fixed cells were washed with PBS three times and dehydrated in gradient concentrations of ethanol (30%, 50%, 70%, 80%, 90%, 95%, and 100%, v/v). Samples were then vacuum-dried at 37 °C for 4 h. Cell attachment on the dried specimens was observed using SEM. In addition, cell spreading and ingrowth were visualized using confocal laser scanning microscopy (CLSM; Nikon). After 12 h of incubation, samples were fixed with 2.5% glutaraldehyde for 15 min, And then cytoskeleton was stained with FITC-phalloidin for 45 min.

2.10.3. Intracellular Nitric Oxide Determination. The intracellular nitric oxide (NO) production of HUVECs was detected by measuring the fluorescence of the probe 3-amino-4-(aminomethyl)-2′,7′-difluorescein, diacetate (DAF-FM DA; Beyotime, Haimen, China) according to the manufacturer's protocol. In short, after HUVECs adhering on PLGA/VEGF and S-PLGA/VEGF scaffolds for 24 h, 500 μL/well DAF-FM DA (5 μM) was dropped onto scaffolds, incubating for 20 min at 37 °C in darkness. Then all specimens were observed using CLSM.

2.10.4. In Vitro Sprouting Analysis. The *in vitro* sprouting analysis was conducted according to a reported protocol.[24] Growth factor reduced Matrigel Matrix was thawed at 4 °C and added into a 96-well microplate on ice (40 μL per well). The 96-well microplate was then transferred to a cell culture incubator and incubated at 37 °C for 30 min to allow Matrigel to gel. The HUVECs that had been cultured for 7 days in experimental groups (negative control, positive control, PLGA/VEGF scaffold, S-PLGA/VEGF scaffold) were trypsinized and then seeded on the gel at a density of 2 × 10^4 cells/well. After incubation for 4 h at 37 °C, the microplate was fixed with 2.5% glutaraldehyde and then examined under an optical microscope. At least five fields were acquired for each substrate, and the total capillary

DOI: 10.1021/acsami.5b02324
ACS Appl. Mater. Interfaces 2015, 7, 9982−9990

tube lengths and number of branch points per field were counted using the NIH ImageJ 1.45 software.

2.11. Statistical Analysis. All quantitative data were expressed as the mean ± standard deviation and were analyzed with Origin 8.5 (OriginLab Corp., Northhampton, MA, USA). Statistical comparisons were carried out using one-way analysis of variance (ANOVA). Statistical significance was attained at greater than the 95% confidence level ($p < 0.05$).

3. RESULTS AND DISCUSSION

3.1. Morphology Observation of Microspheres and Scaffolds. Porous PLGA microspheres were prepared using Pluronic F127 as an extractable porogen in an oil-in-water single emulsion and solvent evaporation process. After removal of F127 by ethanol, the space that F127 once occupied became micropores in the microspheres, which is considered to be beneficial for cellular adhension and nutrient transmission. Furthermore, the topological surface could increase the adsorption of both 26SCS and subsequent growth factor. Figure 1A exhibited both PLGA and S-PLGA microspheres

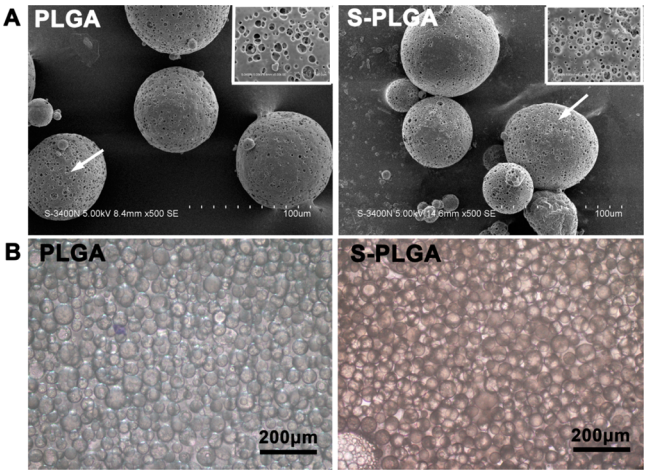

Figure 1. Morphological characterizations of the porous PLGA and S-PLGA microspheres. (A) SEM micrographs of PLGA and S-PLGA microspheres. The insert image at a higher magnification showed topography of the porous surface of the selected area (arrow). (B) Optical micrographs of PLGA and S-PLGA microspheres stained with TB, confirming the presence of heparin-like polysaccharide.

possessing the microstructure of surface perforated and regular spherical particles with diameters of 50−100 μm, indicating that an additional 26SCS-treating did not affect the particle morphology. In addition, positively staining 26SCS-coated microspheres under bright field images presented in Figure 1B demonstrated the presence of sulfated heparin-like polysaccharide.

Cross-section views of microspheres-based scaffolds are shown in Figure 2A. The S-PLGA scaffolds had abundant and interconnected pores among microspheres without obvious variations compared to PLGA scaffolds. Noteworthily, the microsphere-based scaffolds possessed hierarchical porous structure: larger pores of about 50 μm generated by stacking among microspheres, and smaller pores of about 10 μm on the surface of microspheres, owing to the inherent structure of the microspheres. Further SRμCT 3D reconstruction images of the S-PLGA scaffold were created in order to visualize the microstructure of the scaffolds. As indicated in Figure 2B, pore diameters were represented in green; each view of the

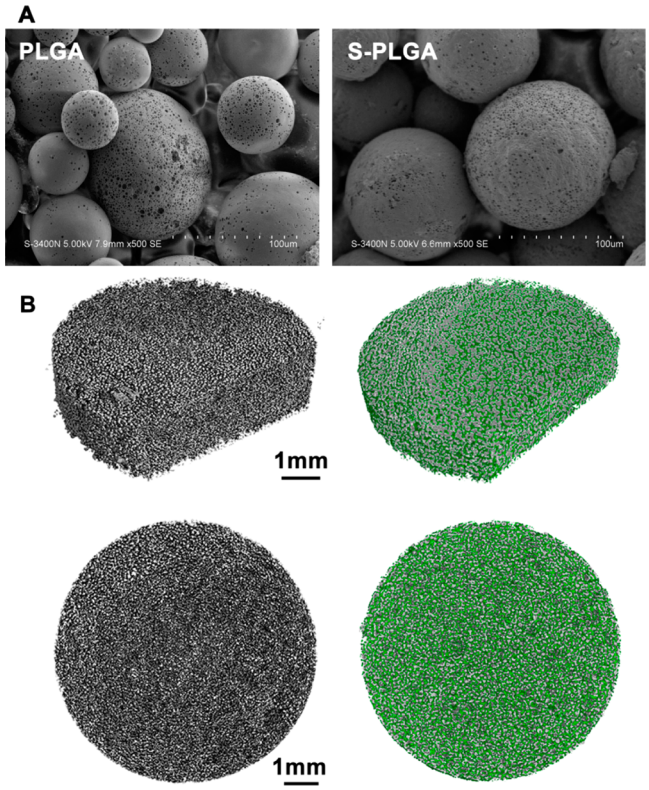

Figure 2. Microstructural analysis of PLGA and S-PLGA scaffolds. (A) SEM micrographs of PLGA and S-PLGA scaffolds. (B) Side view and top view 3D reconstruction image of S-PLGA scaffold with longitudinal section in color (where green areas represent pores among microspheres).

scaffold contained plentiful porous microspheres and the lacunes between the microspheres. The 3D images revealed that PLGA microspheres could be stacked into a structured scaffold through thermal sintering. The average overall porosity of the S-PLGA scaffolds was 71.28 ± 1.79%, and there was no significant difference between the S-PLGA scaffolds and PLGA scaffolds (76.27 ± 5.24%).

3.2. Surface Analysis. Spectra in Figure 3A displayed the elemental photoelectron signals of PLGA and S-PLGA microspheres identified by XPS. As expected, S 2p photoelectron signal was only detected in S-PLGA microsphere; about 2.1 at. % sulfur was detected on the surface of S-PLGA microspheres (Table 1), which was ascribed to the sulfonated modification, demonstrating that 26SCS had been anchored to the surface of S-PLGA microspheres.

The atomic compositions of the PLGA and S-PLGA microspheres surfaces calculated from XPS spectra are listed in Table 1, expressing a slight decrease in the carbon/oxygen (C/O) ratio for S-PLGA (1.34) compared to PLGA (1.52) microspheres. Since the chemical states of the carbon and oxygen atoms in microspheres are key indicators of chemical changes that occur upon the treatments, high-resolution C 1s and O 1s spectra were applied to further characterize the variation of surface elemental compositions of scaffolds. As plotted in Figure 3B, the high-resolution C 1s spectrum of PLGA and S-PLGA microspheres was composed of three peaks: ∼289 eV (O−C═O), ∼287 eV (C−O−C), and ∼285 eV (C−H/C−C), while the decomposition of the O 1s (Figure 3C) envelope revealed the presence of two types of oxygen: O−C at 533.7 eV and O═C at 532.4 eV. The detailed

DOI: 10.1021/acsami.5b02324
ACS Appl. Mater. Interfaces 2015, 7, 9982−9990

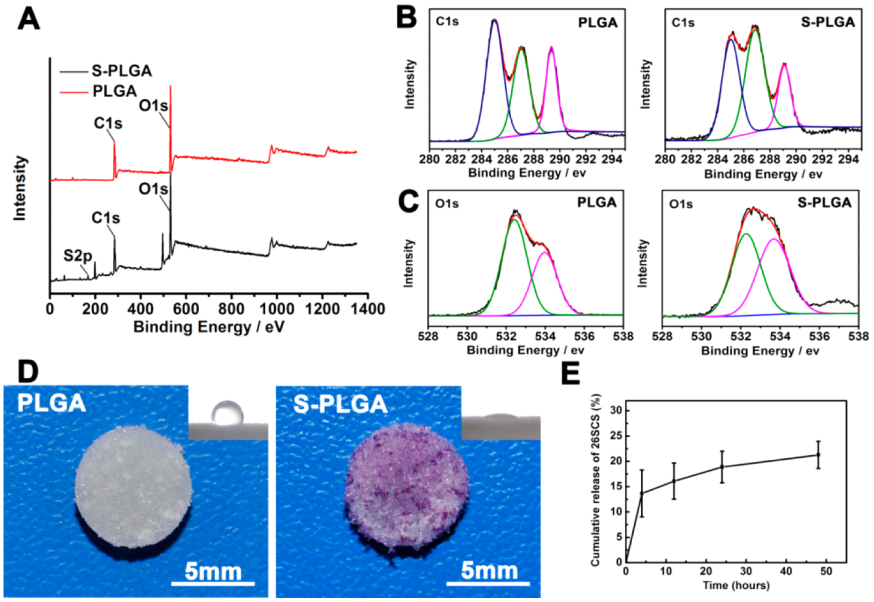

Figure 3. Surface analysis of PLGA and S-PLGA scaffolds. (A) X-ray photoelectron spectroscopy (XPS) patterns of PLGA microspheres and S-PLGA microspheres. (B) XPS spectra of C 1s of PLGA microspheres and S-PLGA microspheres. (C) XPS spectra of O 1s of PLGA microspheres and S-PLGA microspheres. (D) Digital photographs of scaffolds after toluidine blue staining. The insert image showed hydrophilicity of the PLGA and S-PLGA scaffolds. (E) Release kinetics of 26SCS on S-PLGA scaffolds.

Table 1. X-ray Photoelectron Spectroscopy Analysis of PLGA and S-PLGA Microspheres

				envelope ratio (%)				
	elemental ratio (%)			C 1s			O 1s	
sample	C	O	S	C−C/C−H (285.00 eV)	C−O−C (286.85 eV)	O−C═O (289.00 eV)	O═C (532.42 eV)	O−C (533.68 eV)
PLGA	60.3	39.7		45.5	32.3	22.2	60.5	39.5
S-PLGA	56.1	41.8	2.1	38.8	43.9	17.3	49.2	50.8

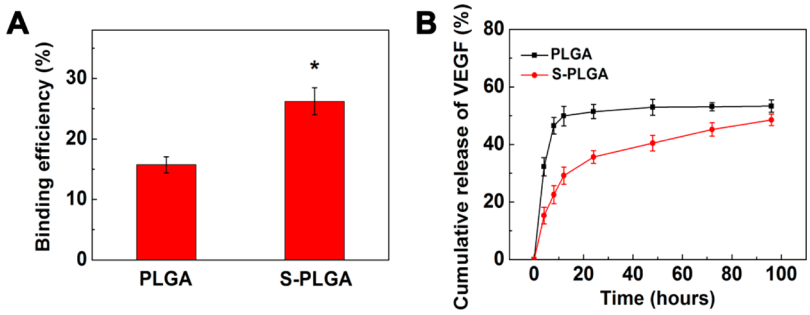

Figure 4. (A) Binding efficiency of VEGF to PLGA and S-PLGA scaffolds. Asterisk indicates significant difference compared to PLGA scaffolds, $p < 0.05$. (B) Release kinetics of VEGF from PLGA/VEGF and S-PLGA/VEGF scaffolds.

parameters listed in Table 1 showed that 32.3% of the C−O−C and 39.5% of the O−C could be detected on the PLGA microsphere, while counts from S-PLGA microspheres increased, reaching 43.9% and 50.8%, respectively. Moreover, PLGA microspheres had an advantage of 22.2% O−C═O and 60.5% O═C compared to the 17.3% O−C═O and 49.2% O═C on S-PLGA microspheres. It could be attributed to 26SCS that contained prolific C−O bonds and less C═O bonds.

The distribution of 26SCS on S-PLGA scaffolds was observed by TB staining as shown in Figure 3D. It was noticeable that there was no color change on PLGA scaffolds after being immersed in TB solution, while uniform distributed purple staining could be seen on the S-PLGA scaffolds. Due to the improved hydrophilicity by introduction of 26SCS, the contact angle of S-PLGA scaffolds (18.8 ± 4.3°) against water was smaller than that of PLGA scaffolds (60.2 ± 1.8°). Distinctive to the superficial modification of scaffolds, the results implied that water-soluble molecules could enter into the S-PLGA microspheres-based scaffolds entirely and incorporate with 26SCS, which was independent of the thickness of the matrix.

The amount of 26SCS immobilized on PLGA scaffolds was further quantitatively determined by TB colorimetric method. There was about 37.4 ± 4.7 $\mu g/cm^3$ 26SCS that could be detected on the S-PLGA scaffolds. In addition, we employed TB to detect 26SCS dissociated from the scaffolds. As depicted in Figure 3E, 26SCS did not appear to have an obvious burst release at the initial stage and manifested a stable liberation throughout the process. It is mainly attributed to the intricate

DOI: 10.1021/acsami.5b02324
ACS Appl. Mater. Interfaces 2015, 7, 9982−9990

and hierarchical pore structure of the scaffold. Due to the outstanding specific surface, the microspheres could easily induce 26SCS to absorb; once the microspheres stacked to form a scaffold, 26SCS could hardly escape from it.

3.3. Binding Efficiency and Release Kinetics of VEGF. The binding efficiency of VEGF to S-PLGA scaffolds was determined and compared to that of PLGA scaffolds, as shown in Figure 4A. With the 26SCS modification, the VEGF binding efficiency of S-PLGA scaffolds was 1.67 fold higher than that of PLGA scaffolds. On account of the meliorative hydrophilicity of S-PLGA scaffolds by introducing 26SCS, VEGF could be easily entrapped into the scaffolds.

Release profiles of VEGF in PLGA/VEGF and S-PLGA/VEGF scaffolds were investigated and plotted in Figure 4B. Both profiles exhibited a typical release curve of physical adsorption, which could be divided into two stages: (a) an initial burst during the first 12 h; (b) a slow steady release during the rest of the time course (12−96 h). The burst release percentage of S-PLGA/VEGF scaffolds during the first 12 h was approximately 30%, while that of PLGA/VEGF scaffolds was up to 50%. Compared to PLGA/VEGF scaffolds, the release of VEGF from S-PLGA/VEGF scaffolds demonstrated sustainable release over the entire time period of the experiment. It is attributed to the high porous structure of the scaffolds, providing a superb accommodation for the loaded VEGF. Furthermore, Ono et al. had reported that the negatively charged *N*- and *O*-sulfated groups of heparin could bind to the basic lysine and arginine residues of VEGF.[31] As a heparin-like polysaccharide, 26SCS contained more *N*- and *O*-sulfated groups to bind to VEGF via spatially matching electrostatic interactions. Besides, 26SCS was difficult to liberate from the surface of microspheres as described earlier. As a result, through binding to 26SCS, decelerated diffusion and promoted local retention of VEGF were successfully realized.

3.4. Angiogenesis Evaluations *in Vitro*. *3.4.1. Cell Viability and Morphology.* The cytotoxicities of PLGA/VEGF and S-PLGA/VEGF scaffolds were evaluated by measuring the mitochondrial metabolic activity of HUVECs cocultured with the scaffolds through a standard MTT assay (Figure 5A). As VEGF is a critical regulatory molecule in cell proliferation, the cell viability on positive control was higher than negative control at every stage, while the VEGF-loaded scaffolds detected a lower cell number at the initial stage which might be induced by cell cytotoxicities of scaffolds and lower VEGF release. Due to the short half-life of VEGF and with the extension of culture time, scaffolds gradually showed their advantages in the capacity of controlled release of growth factor, enhancing the continuous effect of VEGF on endothelial cells. It is mentionable that although PLGA/VEGF scaffolds released more active protein than S-PLGA/VEGF scaffolds at each time, S-PLGA/VEGF scaffolds exhibited better cell viability than PLGA/VEGF scaffolds. Previous work of our group has demonstrated 26SCS stimulated HUVECs to secrete pro-angiogenesis cytokines and promoted neovascularization during bone repairing *in vivo*.[24] Therefore, S-PLGA/VEGF scaffolds are more effective on HUVECs viability than PLGA/VEGF scaffolds at every stage.

In addition, a live/dead assay was used to characterize the visible cellular responses to different scaffolds. As displayed in Figure 5B, fewer dead cells could be observed on S-PLGA/VEGF scaffolds surface than on PLGA/VEGF scaffolds, whereas the live cells on S-PLGA/VEGF scaffolds were more.

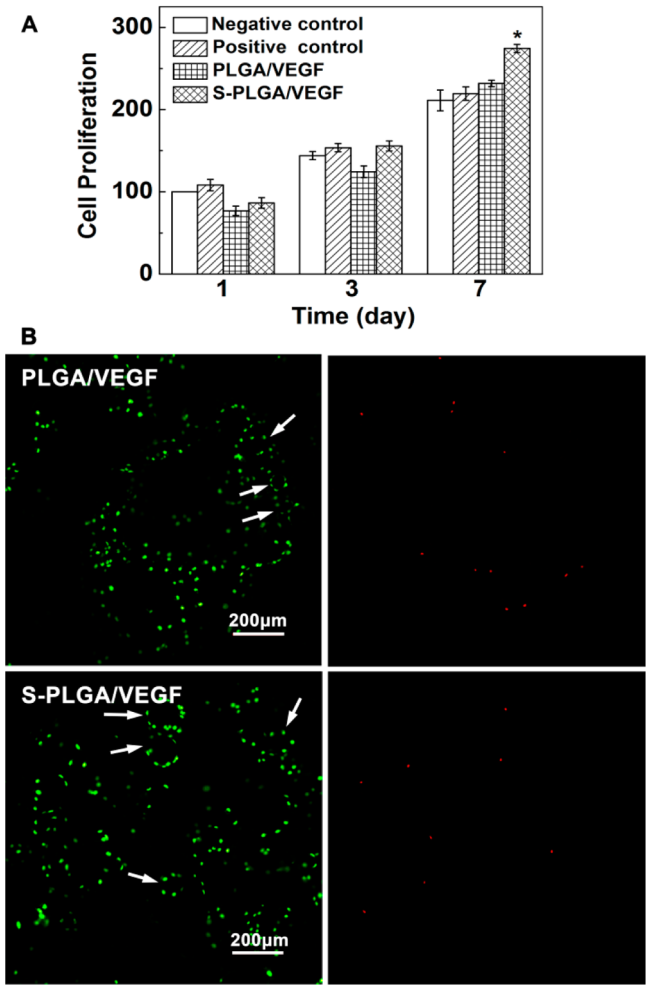

Figure 5. Cell viability of HUVECs on PLGA/VEGF and S-PLGA/VEGF scaffolds. (A) Cell proliferation on the scaffolds after 1, 3, and 7 days determined by MTT assay. The bars represent the percentage of viable cells in the presence of the following: culture medium (negative control), fresh VEGF (10 ng/mL; positive control), PLGA/VEGF scaffolds, and S-PLGA/VEGF scaffolds. Asterisk denotes significant difference ($p < 0.05$) as compared to the negative control group. (B) Live/dead images of HUVECs cultured on PLGA/VEGF scaffolds and S-PLGA/VEGF scaffolds for 24 h showing merge of live and dead cells (left) and dead cells only (right) (white arrow, self-assembly of cells into tubular structures around the microspheres).

Interestingly, the cells residing on scaffolds could self-assemble into tubular structures, indicating that the accumulated spherical structure assisted in guiding HUVECs anchoring and migration, which had a significantly positive effect on pro-angiogenesis *in vitro*.[32]

3.4.2. Cell Attachment and Ingrowth. Cell attachment is the first step of the cell−biomaterial interaction that directly affects the ensuing biological properties. SEM was conducted for detailed cell morphology observation, and initial cell attachment on the scaffolds was evaluated after 12 h cultivation. Figure 6A showed representative microscopy images of cells grown on PLGA and S-PLGA scaffolds. Both scaffolds have a promising potential for cell adhesion which might be attributed to the desirable surface topography. A porous surface improves mechanical interlocking between the biomaterials and the surrounding cells.[33,34] In addition, hierarchical and interconnected structure facilitates nutrients transport and cellular metabolism. However, further survey showed HUVECs spread

DOI: 10.1021/acsami.5b02324
ACS Appl. Mater. Interfaces 2015, 7, 9982−9990

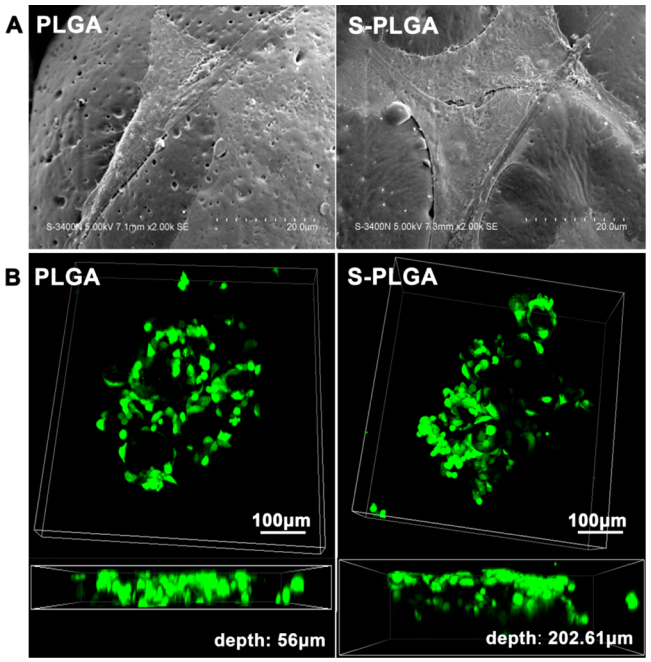

Figure 6. Cell attachment and ingrowth analysis of HUVECs on the surface of scaffolds. (A) SEM images of cell morphology on PLGA scaffolds and S-PLGA scaffolds for 12 h. (B) Confocal laser scanning microscopy: 3D visualization of cell adhesion and ingrowth on PLGA scaffolds and S-PLGA scaffolds.

better with an intimate contact with the surface of the S-PLGA scaffolds, and partially covered the surface of the scaffolds. Cells retained their elongated, spindle-shaped morphology. It has probably contributed to the improved hydrophilicity and roughness of S-PLGA scaffolds with introduced 26SCS.

Furthermore, observation of cell penetration and ingrowth to the scaffolds after 12 h is shown in Figure 6B. The 3D visualization of images revealed that cells anchored with intimate contact along the microspheres with elongated morphologies. Moreover, HUVECs displayed a significant increase in cell ingrowth depth of S-PLGA scaffolds (202.61 μm) compared to the depth of PLGA scaffolds (56 μm).

3.4.3. Intracellular Nitric Oxide Assessment. NO plays an important role in maintenance of vascular homeostasis, as well as regulation of vascular cell proliferation and migration. Thus, the level of intracellular NO production has been used as an important indicator in evaluating vascular function of endothelial cells.[35,36] As evidenced in Figure 7, a higher level of NO secretion was observed on S-PLGA/VEGF scaffolds,

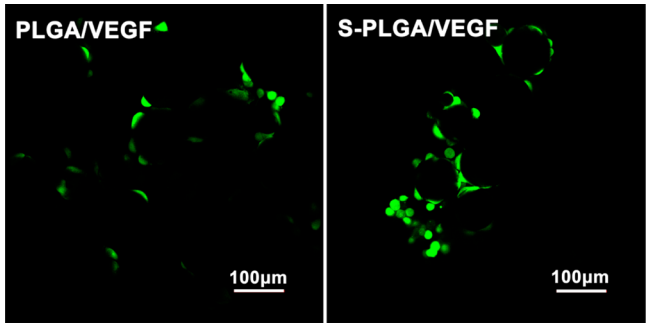

Figure 7. Intracellular NO expression of HUVECs on PLGA/VEGF scaffolds and S-PLGA/VEGF scaffolds.

indicating the ability of S-PLGA/VEGF scaffolds to support the function of NO production. As deduced earlier, two crucial aspects were considered to explicate. Apart from the prolonged and controlled release of VEGF from the S-PLGA/VEGF scaffolds, we considered that the liberated 26SCS had an interaction with VEGF and improved its angiogenic activity via combining with the VEGF receptor 2, which resulted in up-regulation of NO generation.[37,38]

3.4.4. Proangiogenic Activity Evaluation. The angiogenic activity of S-PLGA/VEGF scaffolds was investigated on HUVECs by *in vitro* capillary tube network formation, which was an important process during angiogenesis,[24] and quantified by blinded observer in terms of total capillary tube length and number of branch points per field. As depicted in Figure 8A,

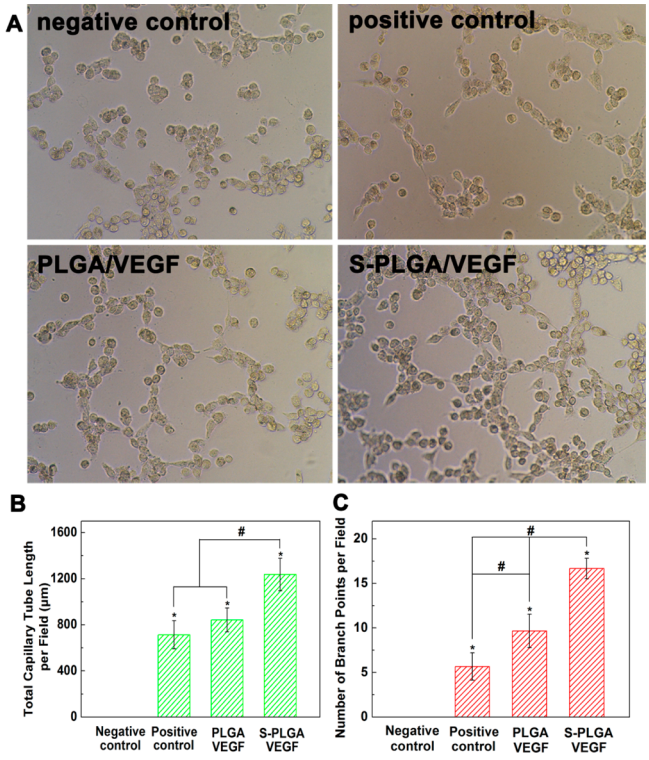

Figure 8. Capillary-like tube formation assay. (A) Representative microscopic images of the capillary network observed in the presence of the following: culture medium (negative control), fresh VEGF (10 ng/mL; positive control), PLGA/VEGF scaffolds, and S-PLGA/VEGF scaffolds. Quantitative analysis of the effects of VEGF-loaded scaffolds on (B) total capillary tube length per field and (C) number of branch points per field of HUVECs capillary-like network. Asterisks (*) and pound symbols (#) denote significant differences ($p < 0.05$) compared to negative control group and between the designated groups, respectively.

without preculture with VEGF, no capillary-like networks of HUVECs were formed on growth factor-reduced Matrigel, while only a few capillary tubes were observed after incubating in positive control. In contrast, capillary-like network formation by HUVECs was obviously observed on both VEGF-containing scaffolds. Particularly, as quantified from the microscopy images, the total capillary tube length per field (Figure 8B) on S-PLGA/VEGF scaffolds was 1.7-fold higher than those cultured on PLGA/VEGF scaffolds ($p < 0.05$). Similarly, compared to PLGA/VEGF scaffolds, the number of branch points per field (Figure 8C) was increased 2.9-fold ($p < 0.05$)

DOI: 10.1021/acsami.5b02324
ACS Appl. Mater. Interfaces 2015, 7, 9982−9990

on S-PLGA/VEGF scaffolds. Actually, VEGF is a potent angiogenic promoter and regarded as a key angiogenic factor that has the strongest and most significant biological activity in enhancing blood vessel formation, stimulating endothelial cells proliferation, migration, survival, and angiogenesis *in vitro*.[10] It was rational to assume that the effect of free VEGF in the positive control was slight due to the rapid depletion of exerted growth factor. Conversely, both PLGA/VEGF and S-PLGA/VEGF scaffolds displayed a longer duration time of VEGF releasing, resulting in vascular tube formation. It is noticed that S-PLGA/VEGF scaffolds have better capability of capillary tube formation, despite the lower VEGF liberation than PLGA/VEGF scaffolds according to the cumulative release profile. By this token, introduction of 26SCS has prominent effects in enhancing pro-angiogenesis activity of VEGF, except for its binding capacity and sustained release of VEGF.

4. CONCLUSIONS

In this study, 26SCS-coated scaffolds with hierarchical structure were developed by accumulation of porous PLGA microspheres. The 26SCS-coating strategy endowed higher affinity between matrix and VEGF. As a consequence, improved loading efficiency and sustained release profile were achieved by S-PLGA scaffolds, as well as better attachment and proliferation of HUVECs. Moreover, S-PLGA/VEGF scaffolds displayed excellent capacity of intracellular NO secretion and capillary-like tube formation which was a prominent process in angiogenesis. These results evidenced that the as-prepared S-PLGA/VEGF scaffolds have the potential to promote angiogenesis, and the 26SCS-coated scaffolds proposed in the study would be a promising delivery vehicle for VEGF.

AUTHOR INFORMATION

Corresponding Authors

*(J.W.) Tel.: +86-21-64251358. Fax: +86-21-64251358. E-mail: biomatwj@163.com.

*(C.L.) Tel.: +86-21-64251358. Fax: +86-21-64251358. E-mail: csliu@sh163.net.

Notes

The authors declare no competing financial interest.

ACKNOWLEDGMENTS

We express our gratitude for the financial support from the National Basic Research Program of China (973 Program, No. 2012CB933600), the National Natural Science Foundation of China (Grant Nos. 31271011, 31330028, and 31470923), and the National Science and Technology Support Program (Grant No, 2012BAI17B02). This study is also supported by New Century Excellent Talents in University (Grant No. NCET-12-0856). Shanghai Synchrotron Radiation Facility is also gratefully acknowledged.

REFERENCES

(1) Tonnesen, M. G.; Feng, X.; Clark, R. A. Angiogenesis in Wound Healing. *J. Invest. Dermatol. Symp. Proc.* **2000**, *5*, 40−46.

(2) Baiguera, S.; Ribatti, D. Endothelialization Approaches for Viable Engineered Tissues. *Angiogenesis* **2013**, *16* (1), 1−14.

(3) Griffith, L. G.; Naughton, G. Tissue Engineering—Current Challenges and Expanding Opportunities. *Science* **2002**, *295* (5557), 1009−1014.

(4) Ko, H. C. H.; Milthorpe, B. K.; McFarland, C. D. Engineering Thick Tissues—The Vascularisation Problem. *Eur. Cells Mater.* **2007**, *14*, 1−18.

(5) Lee, K. Y.; Peters, M. C.; Mooney, D. J. Comparison of Vascular Endothelial Growth Factor and Basic Fibroblast Growth Factor on Angiogenesis in SCID Mice. *J. Controlled Release* **2003**, *87* (1), 49−56.

(6) Sun, G.; Shen, Y.-I.; Kusuma, S.; Fox-Talbot, K.; Steenbergen, C. J.; Gerecht, S. Functional Neovascularization of Biodegradable Dextran Hydrogels with Multiple Angiogenic Growth Factors. *Biomaterials* **2011**, *32* (1), 95−106.

(7) Chen, Y.-C.; Sun, T.-P.; Su, C.-T.; Wu, J.-T.; Lin, C.-Y.; Yu, J.; Huang, C.-W.; Chen, C.-J.; Chen, H.-Y. Sustained Immobilization of Growth Factor Proteins Based on Functionalized Parylenes. *ACS Appl. Mater. Interfaces* **2014**, *6* (24), 21906−21910.

(8) O'Brien, F. J.; Harley, B.; Yannas, I. V.; Gibson, L. J. The Effect of Pore Size on Cell Adhesion in Collagen-GAG Scaffolds. *Biomaterials* **2005**, *26* (4), 433−441.

(9) Zheng, W.; Zhang, W.; Jiang, X. Precise Control of Cell Adhesion by Combination of Surface Chemistry and Soft Lithography. *Adv. Healthcare Mater.* **2013**, *2* (1), 95−108.

(10) Ferrara, N.; Davis-Smyth, T. The Biology of Vascular Endothelial Growth Factor. *Endocr. Rev.* **1997**, *18* (1), 4−25.

(11) Ferrara, N.; Chen, H.; Davis-Smyth, T.; Gerber, H.-P.; Nguyen, T.-N.; Peers, D.; Chisholm, V.; Hillan, K. J.; Schwall, R. H. Vascular Endothelial Growth Factor is Essential for Corpus Luteum Angiogenesis. *Nat. Med.* **1998**, *4* (3), 336−340.

(12) Tayalia, P.; Mooney, D. J. Controlled Growth Factor Delivery for Tissue Engineering. *Adv. Mater.* **2009**, *21* (32−33), 3269−3285.

(13) Lazarous, D. F.; Shou, M.; Scheinowitz, M.; Hodge, E.; Thirumurti, V.; Kitsiou, A. N.; Stiber, J. A.; Lobo, A. D.; Hunsberger, S.; Guetta, E. Comparative Effects of Basic Fibroblast Growth Factor and Vascular Endothelial Growth Factor on Coronary Collateral Development and the Arterial Response to Injury. *Circulation* **1996**, *94* (5), 1074−1082.

(14) Huang, M.; Vitharana, S. N.; Peek, L. J.; Coop, T.; Berkland, C. Polyelectrolyte Complexes Stabilize and Controllably Release Vascular Endothelial Growth Factor. *Biomacromolecules* **2007**, *8* (5), 1607−1614.

(15) Chung, Y.-I.; Kim, S.-K.; Lee, Y.-K.; Park, S.-J.; Cho, K.-O.; Yuk, S. H.; Tae, G.; Kim, Y. H. Efficient Revascularization by VEGF Administration via Heparin-Functionalized Nanoparticle−Fibrin Complex. *J. Controlled Release* **2010**, *143* (3), 282−289.

(16) Carmeliet, P.; Ng, Y.-S.; Nuyens, D.; Theilmeier, G.; Brusselmans, K.; Cornelissen, I.; Ehler, E.; Kakkar, V. V.; Stalmans, I.; Mattot, V. Impaired Myocardial Angiogenesis and Ischemic Cardiomyopathy in Mice Lacking the Vascular Endothelial Growth Factor Isoforms VEGF164 and VEGF188. *Nat. Med.* **1999**, *5* (5), No. 495.

(17) Gerhardt, H.; Golding, M.; Fruttiger, M.; Ruhrberg, C.; Lundkvist, A.; Abramsson, A.; Jeltsch, M.; Mitchell, C.; Alitalo, K.; Shima, D. VEGF Guides Angiogenic Sprouting Utilizing Endothelial Tip Cell Filopodia. *J. Cell Biol.* **2003**, *161* (6), 1163−1177.

(18) Singh, S.; Wu, B. M.; Dunn, J. C. The Enhancement of VEGF-Mediated Angiogenesis by Polycaprolactone Scaffolds with Surface Cross-Linked Heparin. *Biomaterials* **2011**, *32* (8), 2059−2069.

(19) Rostambeigi, N.; Greenlee, S. M.; Huebner, M.; Farley, D. R. When Is the Best Time to Initiate Peri-Operative Heparin Therapy in General Surgery Patients? A Risk-Benefit Dilemma. *Am. Surg.* **2011**, *77* (11), 1539−1545.

(20) Brandner, B.; Kurkela, R.; Vihko, P.; Kungl, A. J. Investigating the Effect of VEGF Glycosylation on Glycosaminoglycan Binding and Protein Unfolding. *Biochem. Biophys. Res. Commun.* **2006**, *340* (3), 836−839.

(21) Gitay-Goren, H.; Soker, S.; Vlodavsky, I.; Neufeld, G. The Binding of Vascular Endothelial Growth Factor to Its Receptors Is Dependent on Cell Surface-Associated Heparin-like Molecules. *J. Biol. Chem.* **1992**, *267* (9), 6093−6098.

(22) Hasan, J.; Shnyder, S. D.; Clamp, A. R.; McGown, A. T.; Bicknell, R.; Presta, M.; Bibby, M.; Double, J.; Craig, S.; Leeming, D. Heparin Octasaccharides Inhibit Angiogenesis in Vivo. *Clin. Cancer Res.* **2005**, *11* (22), 8172−8179.

DOI: 10.1021/acsami.5b02324
ACS Appl. Mater. Interfaces 2015, 7, 9982−9990

(23) Liu, H.; Zhang, Z.; Linhardt, R. J. Lessons Learned from the Contamination of Heparin. *Nat. Prod. Rep.* **2009**, *26* (3), 313−321.
(24) Cao, L.; Wang, J.; Hou, J.; Xing, W.; Liu, C. Vascularization and Bone Regeneration in a Critical Sized Defect Using 2-N, 6-O-Sulfated Chitosan Nanoparticles Incorporating BMP-2. *Biomaterials* **2014**, *35* (2), 684−698.
(25) Anderson, J. M.; Shive, M. S. Biodegradation and Biocompatibility of PLA and PLGA Microspheres. *Adv. Drug Delivery Rev.* **2012**, *64*, 72−82.
(26) Jain, R. A. The Manufacturing Techniques of Various Drug Loaded Biodegradable Poly(lactide-co-glycolide) (PLGA) Devices. *Biomaterials* **2000**, *21* (23), 2475−2490.
(27) Wang, Z.; Chui, W.-K.; Ho, P. C. Design of a Multifunctional PLGA Nanoparticulate Drug Delivery System: Evaluation of Its Physicochemical Properties and Anticancer Activity to Malignant Cancer Cells. *Pharm. Res.* **2009**, *26* (5), 1162−1171.
(28) van de Weert, M.; Hennink, W. E.; Jiskoot, W. Protein Instability in Poly(lactic-co-glycolic acid) Microparticles. *Pharm. Res.* **2000**, *17* (10), 1159−1167.
(29) Zhou, H. J.; Qian, J. C.; Wang, J.; Yao, W. T.; Liu, C. S.; Chen, J. G.; Cao, X. H. Enhanced Bioactivity of Bone Morphogenetic Protein-2 with Low Dose of 2-N, 6-O-Sulfated Chitosan in Vitro and in Vivo. *Biomaterials* **2009**, *30* (9), 1715−1724.
(30) Fisher, J. P. Contrasting Biofunctionalization Strategies for the Enhanced Endothelialization of Biodegradable Vascular Grafts. *Biomacromolecules* **2015**, *16* (2), 437−446.
(31) Ono, K.; Hattori, H.; Takeshita, S.; Kurita, A.; Ishihara, M. Structural Features in Heparin that Interact with VEGF165 and Modulate Its Biological Activity. *Glycobiology* **1999**, *9* (7), 705−711.
(32) Vacharathit, V.; Silva, E. A.; Mooney, D. J. Viability and Functionality of Cells Delivered from Peptide Conjugated Scaffolds. *Biomaterials* **2011**, *32* (15), 3721−3728.
(33) Loh, Q. L.; Choong, C. Three-Dimensional Scaffolds for Tissue Engineering Applications: Role of Porosity and Pore Size. *Tissue Eng., Part B* **2013**, *19* (6), 485−502.
(34) Causa, F.; Netti, P. A.; Ambrosio, L. A Multi-Functional Scaffold for Tissue Regeneration: The Need to Engineer a Tissue Analogue. *Biomaterials* **2007**, *28* (34), 5093−5099.
(35) Wei, Y.; Ji, Y.; Xiao, L.-L.; Lin, Q.-k.; Xu, J.-p.; Ren, K.-f.; Ji, J. Surface Engineering of Cardiovascular Stent with Endothelial Cell Selectivity for in Vivo Re-Endothelialisation. *Biomaterials* **2013**, *34* (11), 2588−2599.
(36) Hoshi, R. A.; Van Lith, R.; Jen, M. C.; Allen, J. B.; Lapidos, K. A.; Ameer, G. The Blood and Vascular Cell Compatibility of Heparin-Modified ePTFE Vascular Grafts. *Biomaterials* **2013**, *34* (1), 30−41.
(37) Olsson, A.-K.; Dimberg, A.; Kreuger, J.; Claesson-Welsh, L. VEGF Receptor Signalling? In Control of Vascular Function. *Nat. Rev. Mol. Cell Biol.* **2006**, *7* (5), 359−371.
(38) Ulissi, Z. W.; Sen, F.; Gong, X.; Sen, S.; Iverson, N.; Boghossian, A. A.; Godoy, L. C.; Wogan, G. N.; Mukhopadhyay, D.; Strano, M. S. Spatiotemporal Intracellular Nitric Oxide Signaling Captured Using Internalized, Near-Infrared Fluorescent Carbon Nanotube Nanosensors. *Nano Lett.* **2014**, *14* (8), 4887−4894.

DOI: 10.1021/acsami.5b02324
ACS Appl. Mater. Interfaces 2015, 7, 9982−9990